Struct Multidisc Optim (2013) 47:317–333
DOI 10.1007/s00158-012-0835-z

RESEARCH PAPER

# Robust topology optimization accounting for misplacement of material

**Miche Jansen · Geert Lombaert · Moritz Diehl · Boyan S. Lazarov · Ole Sigmund · Mattias Schevenels**

Received: 21 December 2011 / Revised: 22 May 2012 / Accepted: 13 August 2012 / Published online: 30 August 2012
© Springer-Verlag 2012

**Abstract** The use of topology optimization for structural design often leads to slender structures. Slender structures are sensitive to geometric imperfections such as the misplacement or misalignment of material. The present paper therefore proposes a robust approach to topology optimization taking into account this type of geometric imperfections. A density filter based approach is followed, and translations of material are obtained by adding a small perturbation to the center of the filter kernel. The spatial variation of the geometric imperfections is modeled by means of a vector valued random field. The random field is conditioned in order to incorporate supports in the design where no misplacement of material occurs. In the robust optimization problem, the objective function is defined as a weighted sum of the mean value and the standard deviation of the performance of the structure under uncertainty. A sampling method is used to estimate these statistics during the optimization process. The proposed method is successfully applied to three example problems: the minimum compliance design of a slender column-like structure and a cantilever beam and a compliant mechanism design. An extensive Monte Carlo simulation is used to show that the obtained topologies are more robust with respect to geometric imperfections.

**Keywords** Topology optimization · Robust design optimization · Geometric imperfections · Random fields

M. Jansen (✉) · G. Lombaert
Department of Civil Engineering, KU Leuven,
Kasteelpark Arenberg 40, 3001 Leuven, Belgium
e-mail: miche.jansen@bwk.kuleuven.be

M. Diehl
Department of Electrical Engineering, KU Leuven,
Kasteelpark Arenberg 10, 3001 Leuven, Belgium

B. S. Lazarov · O. Sigmund
Department of Mechanical Engineering, Solid Mechanics,
Technical University of Denmark, Nils Koppel's Allé,
Building 404, 2800 Lyngby, Denmark

M. Schevenels
Department of Architecture, Urbanism and Planning, KU Leuven,
Kasteelpark Arenberg 1, 3001 Leuven, Belgium

## 1 Introduction

Design optimization has become an intrinsic part of engineering, where high performance designs with a low cost are necessary. Topology optimization is a powerful tool in this respect as it simultaneously optimizes the size, shape and topology of a design, often resulting in new and original designs. This has led to the development of different approaches to topology optimization during the last decades. In this paper, the density based approach (Bendsøe and Sigmund 2004) is adopted.

Topology optimization typically results in designs with a very high performance. The designs obtained by a classical deterministic optimization, however, are often only optimal for a single set of input data and variations in the system can drastically decrease the performance of the design or even make it infeasible. Robust optimization takes these uncertainties into account in the optimization process and searches for well-performing designs that are insensitive with respect to variations in the system. A structure is subjected to multiple sources of uncertainty: loads, material properties, manufacturing errors, environmental conditions, etc. The design of structures under variable loads is a well-known problem in topology optimization. Ben-Tal and Nemirovski (1997) proposed a method to take into account

the worst case load in truss topology optimization by reformulating the minimax problem as a semidefinite program. Brittain et al. (2011) also considered a minimax formulation in continuum topology optimization by explicitly solving the optimality conditions of the worst case load during the optimization. Kogiso et al. (2008) applied a probabilistic approach to model random loads in the design of robust compliant mechanisms. Uncertain material properties have been considered by Asadpoure et al. (2011) in the optimization of truss structures and Chen et al. (2010) applied random fields to model spatially varying material properties in continuum topology optimization.

This paper focuses on geometric imperfections as a source of uncertainty. Two types of geometric imperfections due to manufacturing errors are distinguished: surface imperfections due to over- and under-etching (1) and imperfections due to misplacement or misalignment of material (2). The following distinction is made between these two types of errors. Misplacement (and misalignment) of material indicates that the actual location of the bars of the structure does not correspond to the ideal nominal design. Surface errors due to over- and under-etching on the other hand do not move the structure from its expected position, but instead alter the nominal surface of the design. In other words, misplacement errors cause a perturbation of the location of material in space, while etching errors add or remove material at the surface of the structure.

The first type has already been investigated in the context of topology optimization. Sigmund (2009) and Wang et al. (2011b) proposed a robust optimization method for uniform over- and under-etching errors. A projection step is typically added to density based topology optimization in order to obtain a crisp 0–1 design. Geometric imperfections are modeled by using a variable threshold in the projection step of the optimization process. The uncertain projection threshold is included into the optimization process by means of a worst-case approach. Schevenels et al. (2011) also used a variable projection threshold to model etching errors, but the uncertainties are modeled in a probabilistic sense. In this way, the method could be extended to non-uniform geometric imperfections by means of random field modeling. Chen and Chen (2011) investigated similar imperfections in a level-set approach to topology optimization. In their method, random boundary velocity fields are applied to model the geometric imperfections of the design.

Surface errors often occur due to over- and under-etching during the manufacturing process of micro scale systems such as Micro Electro-Mechanical Systems (MEMS) or waveguides in optical applications (Wang et al. 2011a) and the previous robust methods were mainly applied to the design of this type of systems. Misalignment of material is a typical example of geometric imperfections encountered in structural and civil engineering applications. According to the Eurocodes, this type of imperfections should be accounted for in the design of civil structures (see e.g. Eurocode 3 (1994) for the design of steel structures). The Joint Committee on Structural Safety (JCSS 1999) has proposed probabilistic models for geometric imperfections in braced frames.

Misalignment of material has already been considered in several structural optimization problems. Baitsch and Hartmann (2006) used random perturbations of the nodal locations in order to model geometric imperfections in the shape optimization of truss structures. In truss topology optimization, Guest and Igusa (2008) modeled misalignment of material by perturbing the nodal locations of the ground structure. The imperfections are incorporated into the minimum compliance problem by equivalent nodal forces which are derived from a second order approximation of the nodal perturbations. Jalalpour et al. (2011) added a first order non-linear term to this method in order to account for global instabilities.

This paper proposes a method which incorporates geometric imperfections due to misalignment and misplacement of material into continuum topology optimization. In comparison to the previously discussed methods for shape and topology optimization of trusses, the proposed method does not use variable nodal locations to model misalignment of material. Instead, an Eulerian approach is followed, using a fixed computational grid in the design domain. Perturbation of the material is achieved by shifting the center of the density filter kernel of every element. Density filters are included in continuum topology optimization in order to avoid mesh dependency of the solution and numerical issues such as checkerboards. Furthermore, filters allow the user to control the minimum size of the features in the final design (i.e. they introduce a minimum length into the design). The proposed method only requires a small modification of the density filter in the optimization process in order to model geometric imperfections.

The paper starts with a brief review of density based topology optimization. Afterwards, the perturbed density filter is proposed as a method to model geometric imperfections. A random field model for the spatial variation of geometric imperfections is discussed next. A robust formulation of the optimization problem is applied in order to incorporate the geometric imperfections into the optimization problem. Finally, the method is applied in three examples.

## 2 Topology optimization

### 2.1 Density based approach and SIMP

Continuum topology optimization searches for the best distribution of material in a chosen design domain $\Omega \subset \mathbb{R}^n$.

In the density based approach, the design is represented by the physical densities $\bar{\rho}(\mathbf{x})$ in the design domain. The densities $\bar{\rho}(\mathbf{x})$ are allowed to vary from zero to one where a density equal to zero means void phase and one means solid phase. The continuous design variable $\bar{\rho}(\mathbf{x})$ enables the formulation of smoothly varying functions in the optimization problem. In this way, efficient gradient based algorithms can be applied to solve the optimization problem. The goal of the optimization, however, is to find designs which consist of solid and void phase only (i.e. 0–1 designs) since the intermediate densities have no physical meaning. The solution of the topology optimization problem can be forced to a 0–1 design by means of the Solid Isotropic Material with Penalization (SIMP) method (Bendsøe 1989; Rozvany et al. 1992). The SIMP method makes intermediate densities less efficient in the optimization by using the following density-stiffness interpolation:

$$E(\mathbf{x}) = E_{\min} + (E_0 - E_{\min})\,\bar{\rho}^p(\mathbf{x}) \tag{1}$$

where $p \geq 1$ is the penalization parameter and $E_0$ and $E_{\min}$ are the Young's moduli of respectively the solid and void phase.

The SIMP penalization (i.e. $p > 1$) often leads to ill-posed optimization problems which lack the existence of solution in a continuum formulation. In a discretized finite element setting, numerical problems such as mesh dependency and checkerboards occur (Sigmund and Petersson 1998). Density filters (Bruns and Tortorelli 2001; Bourdin 2001) solve these issues by constraining the space of admissible designs. Density filters are also used to incorporate additional manufacturing requirements such as a minimum length scale into the optimization problem. Modern density filters (Guest et al. 2004; Sigmund 2007; Xu et al. 2010) typically consist of two steps: a smoothing operation and a projection step.

In order to apply a density filter, a new design variable $\rho(\mathbf{x})$ is introduced in the design domain $\Omega$ which will form the optimization variable in the topology optimization problem. The design variable $\rho(\mathbf{x})$ is smoothed by a convolution with a kernel $\kappa(\mathbf{x})$ and the result of this operation is denoted as the intermediate density function $\tilde{\rho}(\mathbf{x})$. The following definition of the density filter is used (Bourdin 2001):

$$\tilde{\rho}(\mathbf{x}) = (\kappa * \rho)(\mathbf{x}) = \frac{\int_{\mathbb{R}^n} \kappa(\mathbf{x}-\mathbf{s})\rho(\mathbf{s})\mathrm{d}\mathbf{s}}{\int_{\mathbb{R}^n} \kappa(\mathbf{x}-\mathbf{s})\mathrm{d}\mathbf{s}} \tag{2}$$

A linear conic function is typically chosen for the kernel function $\kappa(\mathbf{x})$:

$$\kappa(\mathbf{x}) = \max\left(R - \|\mathbf{x}\|_2, 0\right) \tag{3}$$

The filtering radius $R$ reflects the minimum length scale imposed by the designer.

Defining the density filter in this way poses a problem at the boundary of the design domain: the integration in the filter operation is defined over $\mathbb{R}^n$, while the optimization variable $\rho(\mathbf{x})$ is only defined in the design domain $\Omega$. In the literature, this problem is usually solved by self-normalizing the filter operation in the design domain (Sigmund 2007):

$$\tilde{\rho}(\mathbf{x}) = (\kappa * \rho)(\mathbf{x}) = \frac{\int_{\Omega} \kappa(\mathbf{x}-\mathbf{s})\rho(\mathbf{s})\mathrm{d}\mathbf{s}}{\int_{\Omega} \kappa(\mathbf{x}-\mathbf{s})\mathrm{d}\mathbf{s}} \tag{4}$$

In the following, however, formulation (2) is used while assuming that $\rho(\mathbf{x})$ can be extended to $\mathbb{R}^n$ based on the properties of the environment of the problem. For example, at a free Neumann boundary, it can be assumed that there is no material outside the design domain ($\rho = 0$). Likewise, solid material ($\rho = 1$) is placed outside a boundary with Dirichlet conditions assuming that the support consists of material phase.

The smoothing operation limits the space of possible designs $\tilde{\rho}(\mathbf{x})$ and solves the mesh dependency problem. However, the smoothness of the designs $\tilde{\rho}(\mathbf{x})$ also implies gray transition zones at the interface between material and void phases. For this reason, a projection step is added to the density filter which projects intermediate densities $\tilde{\rho}(\mathbf{x})$ by means of a regularized Heaviside function in order to avoid gray zones in the physical design variables $\bar{\rho}(\mathbf{x})$. A continuous approximation of the Heaviside function based on the hyperbolic tangent function is used (Wang et al. 2011b):

$$\bar{\rho}(\mathbf{x}) = \frac{\tanh(\beta\eta) + \tanh\left(\beta\left(\tilde{\rho}(\mathbf{x}) - \eta\right)\right)}{\tanh(\beta\eta) + \tanh\left(\beta\left(1 - \eta\right)\right)} \tag{5}$$

where $\beta$ is a scaling parameter which controls the steepness of the continuous approximation of the Heaviside function and $\eta$ is the threshold value of the Heaviside function. Figure 1 shows the regularized projection function (5) for increasing values of the parameter $\beta$. Although the projection step enables the formation of crisp 0–1 designs, the sensitivities in the topology optimization problem become increasingly ill-conditioned for high values of the parameter $\beta$. For this reason, a continuation scheme on the parameter $\beta$ is usually necessary during the optimization process (see e.g. Andreassen et al. 2011). Alternatively, a fixed high value of $\beta$ can be applied combined with an appropriate rescaling of the trust-region for the primal variable $\rho$ in the optimization algorithm (Guest et al. 2011).

### 2.2 Numerical solution

In the optimization of linear elastic designs, the mechanical problem is solved by means of a finite element discretization of the design domain $\Omega$. The functions $\rho(\mathbf{x})$, $\tilde{\rho}(\mathbf{x})$ and $\bar{\rho}(\mathbf{x})$

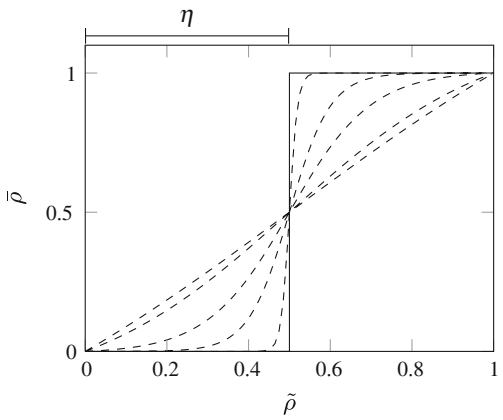


**Fig. 1** Heaviside projection function (*full line*) and continuous projection function (5) (*dashed lines*) with a projection threshold $\eta = 0.5$ and increasing values of the parameter $\beta$

are discretized to a constant value $\rho_e$, $\tilde{\rho}_e$ and $\bar{\rho}_e$ per finite element. These element values are collected in the vectors $\boldsymbol{\rho}$, $\tilde{\boldsymbol{\rho}}$ and $\bar{\boldsymbol{\rho}}$.

The state of the system is represented by the nodal displacement vector $\mathbf{u}(\boldsymbol{\rho})$ which can be calculated by means of the finite element equilibrium equations:

$$\mathsf{K}(\boldsymbol{\rho})\mathbf{u}(\boldsymbol{\rho}) - \mathbf{f} = \mathbf{0} \tag{6}$$

where $\mathsf{K}(\boldsymbol{\rho})$ is the global stiffness matrix and $\mathbf{f}$ the vector of nodal loads. The global stiffness matrix is assembled from the element stiffness matrices $\mathsf{K}_e(\boldsymbol{\rho})$ which depend linearly on the elements' Young's moduli: $\mathsf{K}_e(\boldsymbol{\rho}) = E_e(\boldsymbol{\rho})\mathsf{K}_e^0$, with $\mathsf{K}_e^0$ the element matrix for a Young's modulus equal to one.

The convolution in the density filter is replaced by a discrete convolution. The self-normalizing filter (4) is approximated by:

$$\tilde{\rho}_e = (\boldsymbol{\kappa} * \boldsymbol{\rho})_e = \frac{\sum_{j\in Q^e} \kappa(\mathbf{x}_e - \mathbf{x}_j) v_j \rho_j}{\sum_{j\in Q^e} \kappa(\mathbf{x}_e - \mathbf{x}_j) v_j} \tag{7}$$

where $v_j$ are the element volumes and $\mathbf{x}_e$ the location of the element centers. The neighborhood $Q^e$ is the index set of all elements within a distance $R$ to element $e$:

$$Q^e = \{i \in 1, \ldots, n_\mathrm{e} | \|\mathbf{x}_e - \mathbf{x}_i\|_2 \leq R\} \tag{8}$$

where $n_\mathrm{e}$ is the total number of elements in the design domain.

In order to discretize the filter (2), we have to assume that we know the extension of $\boldsymbol{\rho}$ beyond the boundaries of the design domain $\Omega$. The discretization of (2) can then be defined in the following way:

$$\tilde{\rho}_e = (\boldsymbol{\kappa} * \boldsymbol{\rho})_e = \frac{\sum_{j\in \bar{Q}^e} \kappa(\mathbf{x}_e - \mathbf{x}_j) v_j \rho_j}{\sum_{j\in \bar{Q}^e} \kappa(\mathbf{x}_e - \mathbf{x}_j) v_j} \tag{9}$$

where $\bar{Q}^e$ is the extended neighborhood which also contains the contributions of the extension of $\boldsymbol{\rho}$ outside $\Omega$.

### 2.3 Optimization problem

This paper considers the minimum compliance problem and the optimal design of compliant mechanisms. Both problems can be formulated in the following way:

$$\begin{aligned} \min_{\boldsymbol{\rho}} \ & f(\boldsymbol{\rho}) = \mathbf{b}^\mathrm{T}\mathbf{u}(\boldsymbol{\rho}) \\ \text{s.t. } & V(\boldsymbol{\rho}) - V_\mathrm{max} \leq 0 \\ & \mathbf{0} \leq \boldsymbol{\rho} \leq \mathbf{1} \end{aligned} \tag{10}$$

where $\mathbf{b}$ is a vector depending on the nature of the problem and $V(\boldsymbol{\rho})$ is the volume fraction of the design domain occupied by the physical densities $\bar{\boldsymbol{\rho}}$:

$$V(\boldsymbol{\rho}) = \frac{\sum_{j=1}^{n_\mathrm{e}} v_j \bar{\rho}_j}{\sum_{j=1}^{n_\mathrm{e}} v_j} \tag{11}$$

The goal of the minimum compliance problem is to minimize the work done by the external forces while the volume of the design is limited to a certain volume fraction $V_\mathrm{max}$ of the domain $\Omega$. In this case, the vector $\mathbf{b}$ is equal to the external load vector $\mathbf{f}$. In the compliant mechanism design problem, an output displacement component $u_\mathrm{out}$ is maximized. The output displacement is selected from $\mathbf{u}$ by an appropriate choice of the vector $\mathbf{b}$.

The sensitivities of the objective function $f(\boldsymbol{\rho})$ with respect to the physical densities $\bar{\rho}_e$ are calculated using the adjoint method:

$$\frac{\partial f(\boldsymbol{\rho})}{\partial \bar{\rho}_e} = -\boldsymbol{\lambda}^\mathrm{T} \frac{\partial \mathsf{K}}{\partial \bar{\rho}_e}\mathbf{u} \tag{12}$$

where $\lambda$ is the adjoint vector which solves the adjoint system $\mathsf{K}\boldsymbol{\lambda} = \mathbf{b}$. The chain rule of differentiation is applied twice to obtain the sensitivities with respect to the actual optimization variables $\rho_e$:

$$\frac{\partial f}{\partial \rho_e} = \sum_{i\in Q^e} \frac{\partial f}{\partial \bar{\rho}_i} \frac{\partial \bar{\rho}_i}{\partial \tilde{\rho}_i} \frac{\partial \tilde{\rho}_i}{\partial \rho_e} \tag{13}$$

The intermediate derivatives follow from differentiation of the projection function (5) and the density filter (9):

$$\frac{\partial \bar{\rho}_i}{\partial \tilde{\rho}_i} = \frac{\beta\,(\mathrm{sech}\,(\beta(\tilde{\rho}_i - \eta)))^2}{\tanh(\beta\eta) + \tanh\,(\beta(1-\eta))} \tag{14}$$

$$\frac{\partial \tilde{\rho}_i}{\partial \rho_e} = \frac{\kappa(\mathbf{x}_i - \mathbf{x}_e) v_e}{\sum_{j\in \bar{Q}^i} \kappa(\mathbf{x}_i - \mathbf{x}_j) v_j} \tag{15}$$

The sensitivities of the volume constraint are calculated similarly by applying the chain rule twice.

## 3 Modeling geometrical imperfections

### 3.1 Misplacement and misalignment of material

A perturbation of the structural members in a design can be modeled by considering the nodal locations in the computational model (i.e. finite element model) as variables subjected to uncertainty. This approach has for example been successfully applied to model geometric imperfections in robust shape optimization problems (Baitsch and Hartmann 2006) and robust truss topology optimization problems (Guest and Igusa 2008). Such an approach can be denoted as a Lagrangian type method since the computational grid (i.e. finite element mesh) follows the geometry of the design.

Varying the computational grid is obviously also applicable to continuum topology optimization problems. Whereas many shape optimization methods consider Lagrangian grids to describe the design, a fixed Eulerian framework is considered in topology optimization. It therefore seems appropriate to model the geometric imperfections on the same fixed computational grid.

Inspired by the work of Schevenels et al. (2011) where geometric imperfections due to over- and under-etching are modeled by adding a random component to the projection step in (5) of the density filter, we propose to model misalignment of material by means of a random component in the smoothing operation in (2) of the density filter.

A vector valued random field $\mathbf{p}(\mathbf{x},\theta) : \Omega \times \mathcal{A} \rightarrow \mathbb{R}^n$ is introduced in order to model the geometric imperfections. In agreement with Kolmogorov's probability theory (Kolmogorov 1956), a random variable or field is denoted as a function of the probabilistic elementary event $\theta$ of the event space $\mathcal{A}$. Section 3.2 elaborates on the random field model $\mathbf{p}(\mathbf{x},\theta)$, but first we will discuss how the random perturbation is incorporated into the topology optimization problem in order to model geometric imperfections.

The misplacement of material is modeled by adding the random perturbation vector $\mathbf{p}(\mathbf{x},\theta)$ to the center of the filter kernel. The density filter (2) is modified in the following way:

$$\tilde{\rho}(\mathbf{x}|\mathbf{p}(\mathbf{x},\theta)) = (\kappa * \rho)(\mathbf{x} - \mathbf{p}(\mathbf{x},\theta)) \tag{16}$$

Figure 2 illustrates the modification of the density filter in (16) when the linear filter kernel in (3) is used. In the nominal case (Fig. 2a) the filter kernel is centered around the centroid of the finite element and $\tilde{\rho}_e$ is determined by the element densities $\rho$ in the neighborhood $Q^e$. When the perturbation $\mathbf{p}(\mathbf{x},\theta)$ is added to the density filter (Fig. 2b), $\tilde{\rho}_e$ is determined by the densities $\rho$ of the neighborhood of a shifted location. In other words, the geometric imperfections are modeled by slightly perturbing the mapping from $\boldsymbol{\rho}$ to $\tilde{\boldsymbol{\rho}}$. The effect of the perturbed density filter is illustrated in Fig. 3. The primal densities $\boldsymbol{\rho}$ represent a grid-like structure without imperfections. Next, three realizations of the random field $\mathbf{p}(\mathbf{x},\theta)$ are generated which are shown in the second row of Fig. 3. These imperfections are incorporated by means of the perturbed density filter in (16). The third row shows the smoothed and perturbed intermediate densities $\tilde{\boldsymbol{\rho}}$. The resulting physical densities $\bar{\boldsymbol{\rho}}$ in the fourth row of Fig. 3 contain bars which are clearly misaligned.

### 3.2 Random field representation

The spatial variation of the perturbation vector is modeled by means of the Gaussian random field $\mathbf{p}(\mathbf{x},\theta)$ in design domain $\Omega$. A Gaussian random field is fully characterized by a mean function and a covariance function. The mean function $\mathbf{m_p}(\mathbf{x})$ is defined as:

$$\mathbf{m_p}(\mathbf{x}) = \mathbb{E}\left[\mathbf{p}(\mathbf{x},\theta)\right] \tag{17}$$

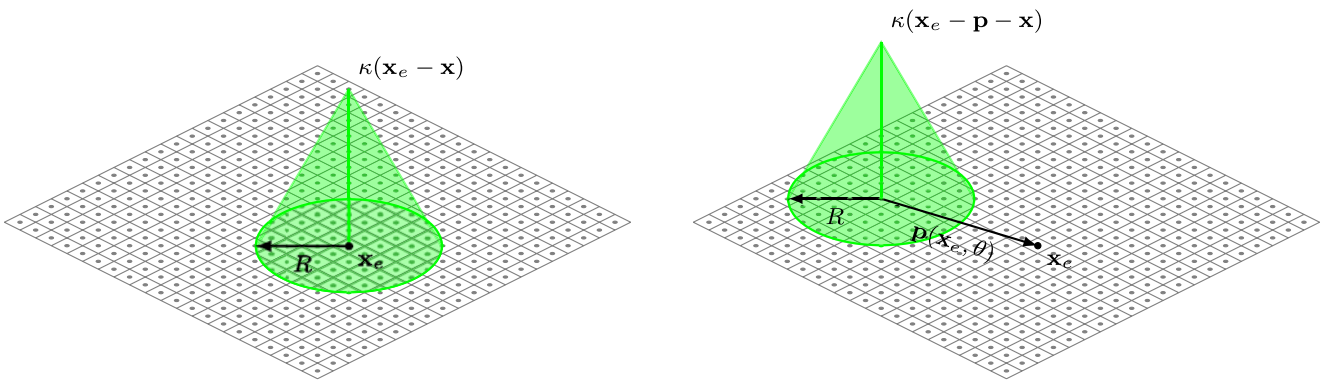


(a) Density filter (b) Perturbed density filter

**Fig. 2** Translation of material by a perturbation of the center of the filter kernel in $\mathbb{R}^2$

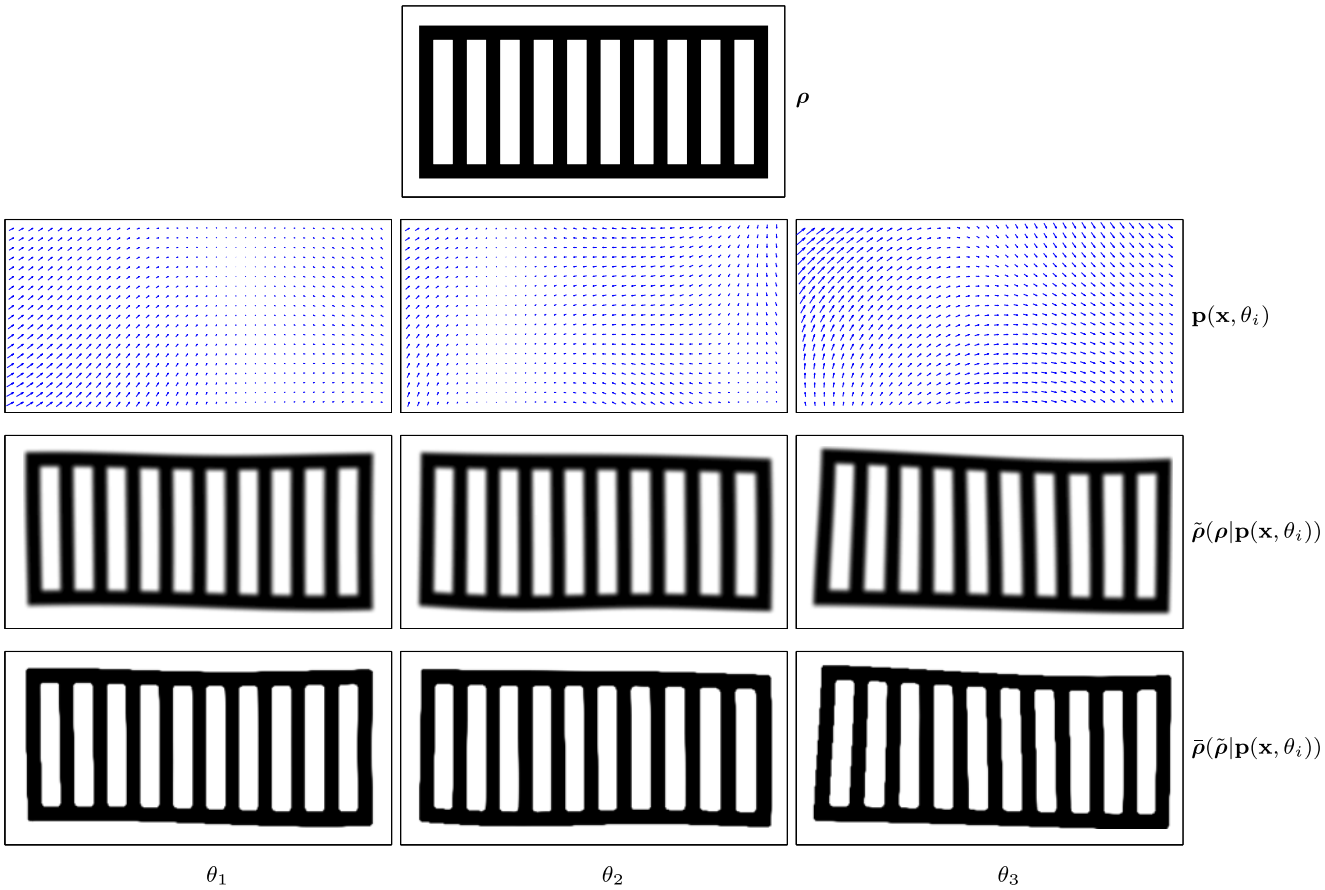


**Fig. 3** Example of spatially varying geometrical imperfections by means of the random field $\mathbf{p}(\mathbf{x}, \theta)$. The design variables $\boldsymbol{\rho}$, the filtered variables $\tilde{\boldsymbol{\rho}}(\boldsymbol{\rho}|\mathbf{p}(\mathbf{x}, \theta))$ and the projected variables $\bar{\boldsymbol{\rho}}(\tilde{\boldsymbol{\rho}}|\mathbf{p}(\mathbf{x}, \theta))$ obtained for three samples of the random field $\mathbf{p}(\mathbf{x}, \theta_i)$

where $\mathbb{E}$ is the expectation operator. Since $\mathbf{p}(\mathbf{x}, \theta)$ is a random vector field, the covariance function $\mathsf{C}_{\mathbf{p}}(\mathbf{x}_1, \mathbf{x}_2) : \mathbb{R}^n \times \mathbb{R}^n \to \mathbb{R}^{n \times n}$ is a matrix valued function:

$$\begin{aligned}\mathsf{C}_{\mathbf{p}}(\mathbf{x}_1, \mathbf{x}_2) &= \mathrm{Cov}\left[\mathbf{p}(\mathbf{x}_1, \theta), \mathbf{p}(\mathbf{x}_2, \theta)\right] \\ &= \mathbb{E}\left[\left(\mathbf{p}(\mathbf{x}_1, \theta) - \mathbf{m}_{\mathbf{p}}(\mathbf{x}_1)\right)\left(\mathbf{p}(\mathbf{x}_2, \theta) - \mathbf{m}_{\mathbf{p}}(\mathbf{x}_2)\right)^{\mathrm{T}}\right]\end{aligned} \tag{18}$$

Since the imperfections are expected to be symmetric with respect to the nominal design, the mean is chosen $\mathbf{m}_{\mathbf{p}} = \mathbf{0}$.

Moreover, only random fields with the principal axes parallel to the coordinate axes are considered here. In this case, the covariance function is a diagonal matrix, e.g. in $\mathbb{R}^2$:

$$\mathsf{C}_{\mathbf{p}}(\mathbf{x}_1, \mathbf{x}_2) = \begin{bmatrix} C_{\mathrm{p}_1}(\mathbf{x}_1, \mathbf{x}_2) & 0 \\ 0 & C_{\mathrm{p}_2}(\mathbf{x}_1, \mathbf{x}_2) \end{bmatrix} \tag{19}$$

where $C_{\mathrm{p}_i}(\mathbf{x}_1, \mathbf{x}_2)$ is the covariance function of the component $p_i(\mathbf{x}, \theta)$ of the random field $\mathbf{p}(\mathbf{x}, \theta)$. Due to this assumption, the components of the random field are uncorrelated and independent which means that every component of the random field can be modeled as a separate scalar-valued random field. A squared exponential covariance function is used for the components $p_i(\mathbf{x}, \theta)$ of the random field:

$$C_{\mathrm{p}_i}(\mathbf{x}_1, \mathbf{x}_2) = \sigma_{\mathrm{p}_i}^2 \exp\left[-\left(\left(\frac{x_1 - x_2}{l_{\mathrm{c}x}}\right)^2 + \left(\frac{y_1 - y_2}{l_{\mathrm{c}y}}\right)^2\right)\right] \tag{20}$$

where $\sigma_{\mathrm{p}_i}$ is the standard deviation of the component $p_i$ of the random field and $l_{\mathrm{c}x}$ and $l_{\mathrm{c}y}$ are the correlation lengths of the random field in the coordinate directions $x$ and $y$.

### 3.3 Random fields with known values

It is reasonable to assume that the magnitude of the geometrical imperfections decreases close to the supports of the structure. Furthermore, since the design should always satisfy the kinematic boundary conditions, the random field should have a fixed value at the supports. These assumptions can be accounted for using a conditioned random field based on random field interpolation using linear regression (Ditlevsen 1996). This approach has been applied by several authors to model random fields of geometrical

imperfections (Baitsch and Hartmann 2006; Kolanek and Jendo 2008). In the Gaussian case, the method is equivalent to replacing the random field by a conditional random field with known values. Assuming there is a set of points $\{\bar{\mathbf{x}}_i \in \Omega | i \in 1, \ldots, m\}$ where the value of the random field is fixed, the covariance function $\mathsf{C}_{\mathbf{p}}(\mathbf{x}_1, \mathbf{x}_2)$ is replaced by the conditional covariance function $\tilde{\mathsf{C}}_{\mathbf{p}}(\mathbf{x}_1, \mathbf{x}_2)$:

$$\begin{aligned}\tilde{\mathsf{C}}_{\mathbf{p}}(\mathbf{x}_1, \mathbf{x}_2) &= \mathrm{Cov}\left[\mathbf{p}(\mathbf{x}_1, \theta), \mathbf{p}(\mathbf{x}_2, \theta) | \mathbf{p}(\bar{\mathbf{x}}_i, \theta) = 0\right] \\ &= \mathsf{C}_{\mathbf{p}}(\mathbf{x}_1, \mathbf{x}_2) - \mathsf{C}^{\mathrm{T}}_{\mathbf{p}\bar{\mathbf{p}}}(\mathbf{x}_1)\mathsf{C}^{-1}_{\bar{\mathbf{p}}\bar{\mathbf{p}}}\mathsf{C}_{\mathbf{p}\bar{\mathbf{p}}}(\mathbf{x}_2)\end{aligned} \tag{21}$$

with:

$$\mathsf{C}_{\mathbf{p}\bar{\mathbf{p}}}(\mathbf{x}) = \begin{bmatrix} \mathsf{C}_{\mathbf{p}}(\mathbf{x}, \bar{\mathbf{x}}_1) \\ \vdots \\ \mathsf{C}_{\mathbf{p}}(\mathbf{x}, \bar{\mathbf{x}}_m) \end{bmatrix} \tag{22}$$

and:

$$\mathsf{C}_{\bar{\mathbf{p}}\bar{\mathbf{p}}} = \begin{bmatrix} \mathsf{C}_{\mathbf{p}}(\bar{\mathbf{x}}_1, \bar{\mathbf{x}}_1) & \cdots & \mathsf{C}_{\mathbf{p}}(\bar{\mathbf{x}}_1, \bar{\mathbf{x}}_m) \\ \vdots & \ddots & \vdots \\ \mathsf{C}_{\mathbf{p}}(\bar{\mathbf{x}}_m, \bar{\mathbf{x}}_1) & \cdots & \mathsf{C}_{\mathbf{p}}(\bar{\mathbf{x}}_m, \bar{\mathbf{x}}_m) \end{bmatrix} \tag{23}$$

### 3.4 The EOLE method for random field discretization

The random field is discretized with the Expansion Optimal Linear Estimation method (EOLE) (Li and Der Kiureghian 1993). The method can be summarized as follows for a Gaussian random field. First, a finite subset of points $\left\{\hat{\mathbf{x}}_i \in \Omega | i = 1, \ldots, k\right\}$ is chosen. These points can be selected on either a structured or an unstructured grid in $\Omega$. Due to the Gaussianity of the random field, the vector $\mathbf{Z}(\theta) \in \mathbb{R}^{kn}$ is a Gaussian random vector:

$$\mathbf{Z}(\theta) = \begin{Bmatrix} \mathbf{p}(\hat{\mathbf{x}}_1, \theta) \\ \vdots \\ \mathbf{p}(\hat{\mathbf{x}}_k, \theta) \end{Bmatrix} \tag{24}$$

The covariance matrix $\tilde{\mathsf{C}}_{\mathbf{ZZ}} \in \mathbb{R}^{kn \times kn}$ of $\mathbf{Z}(\theta)$ is:

$$\tilde{\mathsf{C}}_{\mathbf{ZZ}} = \begin{bmatrix} \tilde{\mathsf{C}}_{\mathbf{p}}(\hat{\mathbf{x}}_1, \hat{\mathbf{x}}_1) & \cdots & \tilde{\mathsf{C}}_{\mathbf{p}}(\hat{\mathbf{x}}_1, \hat{\mathbf{x}}_k) \\ \vdots & \ddots & \vdots \\ \tilde{\mathsf{C}}_{\mathbf{p}}(\hat{\mathbf{x}}_k, \hat{\mathbf{x}}_1) & \cdots & \tilde{\mathsf{C}}_{\mathbf{p}}(\hat{\mathbf{x}}_k, \hat{\mathbf{x}}_k) \end{bmatrix} \tag{25}$$

The random vector $\mathbf{Z}(\theta)$ is decorrelated using the spectral representation of the covariance matrix $\tilde{\mathsf{C}}_{\mathbf{ZZ}}$:

$$\mathbf{Z}(\theta) = \sum_{i=1}^{kn} \sqrt{\lambda_i}\mathbf{v}_i \xi_i(\theta) \tag{26}$$

where $\xi_i(\theta)$ are independent standard normal variables and $\lambda_i$ and $\mathbf{v}_i$ the eigenvalues and eigenvectors of the covariance matrix $\tilde{\mathsf{C}}_{\mathbf{ZZ}}$:

$$\tilde{\mathsf{C}}_{\mathbf{ZZ}}\mathbf{v}_i = \lambda_i \mathbf{v}_i \tag{27}$$

Next, linear regression (Ditlevsen 1996) is applied to obtain an approximation of the random field as a function of the random vector $\mathbf{Z}(\theta)$. The linear regression of the random field at point $\mathbf{x} \in \Omega$ on vector $\mathbf{Z}(\theta)$ is given by:

$$\mathbf{p}(\mathbf{x}, \theta) \approx \tilde{\mathsf{C}}^{\mathrm{T}}_{\mathbf{pZ}}(\mathbf{x})\tilde{\mathsf{C}}^{-1}_{\mathbf{ZZ}}\mathbf{Z}(\theta) \tag{28}$$

where $\tilde{\mathsf{C}}_{\mathbf{pZ}}(\mathbf{x}) \in \mathbb{R}^{kn \times n}$ is the covariance matrix of $\mathbf{Z}(\theta)$ and $\mathbf{p}(\mathbf{x}, \theta)$:

$$\tilde{\mathsf{C}}_{\mathbf{pZ}}(\mathbf{x}) = \begin{bmatrix} \tilde{\mathsf{C}}_{\mathbf{p}}(\mathbf{x}, \hat{\mathbf{x}}_1) \\ \vdots \\ \tilde{\mathsf{C}}_{\mathbf{p}}(\mathbf{x}, \hat{\mathbf{x}}_k) \end{bmatrix} \tag{29}$$

Finally, the spectral decomposition (26) is introduced into (28) resulting in the EOLE approximation of the random field:

$$\begin{aligned}\mathbf{p}(\mathbf{x}, \theta) &\approx \tilde{\mathsf{C}}^{\mathrm{T}}_{\mathbf{pZ}}(\mathbf{x})\tilde{\mathsf{C}}^{-1}_{\mathbf{ZZ}}\mathbf{Z}(\theta) \\ &= \sum_{i=1}^{kn} \frac{1}{\lambda_i}\tilde{\mathsf{C}}^{\mathrm{T}}_{\mathbf{pZ}}(\mathbf{x})\mathbf{v}_i\mathbf{v}_i^{\mathrm{T}}\mathbf{Z}(\theta) \\ &= \sum_{i=1}^{kn} \frac{1}{\sqrt{\lambda_i}}\tilde{\mathsf{C}}^{\mathrm{T}}_{\mathbf{pZ}}(\mathbf{x})\mathbf{v}_i\xi_i(\theta) \\ &= \sum_{i=1}^{kn} \boldsymbol{\varphi}_i(\mathbf{x})\xi_i(\theta)\end{aligned} \tag{30}$$

Similar to the Karhunen–Loève decomposition, the expansion (30) can be truncated at a number $r < kn$, keeping only the most important random components in the approximation.

Sudret and Der Kiureghian (2000) have performed a parametric study of the number of points $k$. A distance between the points smaller than $l_c/2$ to $l_c/3$ is recommended for the squared exponential covariance function (20). A relatively small number of points is required in case of a large correlation length and therefore an eigenvalue problem (27) with a relatively small dimension has to be solved. For this reason, the EOLE method is particularly well suited for discretizing random fields with a relatively large correlation length.

## 4 Robust optimization problem

### 4.1 Formulation of the optimization problem

Using the EOLE representation of the random field, the physical densities $\bar{\boldsymbol{\rho}}(\boldsymbol{\rho}, \boldsymbol{\xi}) = \bar{\boldsymbol{\rho}}(\tilde{\boldsymbol{\rho}}(\boldsymbol{\rho}, \boldsymbol{\xi}))$ can be expressed as a function of a discrete set of random variables $\boldsymbol{\xi}$ and the optimization variables $\boldsymbol{\rho}$. The state variables $\mathbf{u}(\boldsymbol{\rho}, \boldsymbol{\xi})$ are described as a function of $\boldsymbol{\xi}$ and $\boldsymbol{\rho}$ by means of the stochastic equilibrium equations:

$$\mathsf{K}(\boldsymbol{\rho}, \boldsymbol{\xi})\mathbf{u}(\boldsymbol{\rho}, \boldsymbol{\xi}) - \mathbf{f}(\boldsymbol{\xi}) = \mathbf{0} \tag{31}$$

Consequently, the compliance $f(\boldsymbol{\rho}, \boldsymbol{\xi}) = \mathbf{f}^{\mathrm{T}}(\boldsymbol{\xi})\mathbf{u}(\boldsymbol{\rho}, \boldsymbol{\xi})$ also depends on the random variables $\boldsymbol{\xi}$.

In the following examples, it is assumed that the location of the load $\mathbf{f}(\boldsymbol{\xi})$ depends on the geometric imperfections for two reasons. The loads on a structure are usually applied after the structure has been built and therefore their location changes in the same way as the structure. If the position of the load is fixed, the objective function would become a highly non-linear function of the geometric imperfections, since the load would 'fall off' the structure at a certain level of perturbation resulting in very high values of compliance.

The goal of robust optimization is to find designs with a good performance that are also insensitive with respect to small variations in the system. Multiple formulations of robust optimization problems exist in the literature mainly differing in which measure of robustness is chosen and how the uncertainties are modeled (e.g. by means of probabilistic modeling, convex sets, or fuzzy modeling). Beyer and Sendhoff (2007) have made a thorough survey of the existing approaches to robust optimization. In the present work, a probabilistic approach is followed as it permits to model the geometric imperfections in a rigorous way using random field theory. A common approach to robust optimization in a probabilistic setting is to measure the robustness of the design by means of the mean performance $m_f(\boldsymbol{\rho})$ and the standard deviation $\sigma_f(\boldsymbol{\rho})$ of the performance:

$$m_f(\boldsymbol{\rho}) = \mathbb{E}\left[f(\boldsymbol{\rho}, \boldsymbol{\xi})\right] \tag{32}$$

$$\sigma_f(\boldsymbol{\rho}) = \sqrt{\mathbb{E}\left[\left(f(\boldsymbol{\rho}, \boldsymbol{\xi})\right)^2 - \left(m_f(\boldsymbol{\rho})\right)^2\right]} \tag{33}$$

In the robust optimization problem, the objective function is replaced by a weighted sum of the mean and the standard deviation of the performance:

$$\begin{aligned} &\min_{\boldsymbol{\rho}} \; m_f(\boldsymbol{\rho}) + \omega\sigma_f(\boldsymbol{\rho}) \\ &\text{s.t. } V(\boldsymbol{\rho}) - V_{\max} \leq 0 \\ &\quad \mathbf{0} \leq \boldsymbol{\rho} \leq \mathbf{1} \end{aligned} \tag{34}$$

The volume constraint is imposed on the nominal design. The parameter $\omega$ represents a trade-off between an optimal mean performance and a small variance of the performance of the design.

Using the linearity of the expectation operator the sensitivities of the robust objective function can be written as:

$$\frac{\partial m_f(\boldsymbol{\rho})}{\partial \rho_e} = \frac{\partial \mathbb{E}\left[f(\boldsymbol{\rho}, \boldsymbol{\xi})\right]}{\partial \rho_e} = \mathbb{E}\left[\frac{\partial f(\boldsymbol{\rho}, \boldsymbol{\xi})}{\partial \rho_e}\right] \tag{35}$$

$$\frac{\partial \sigma_f(\boldsymbol{\rho})}{\partial \rho_e} = \frac{1}{\sigma_f(\boldsymbol{\rho})}\mathbb{E}\left[\left(f(\boldsymbol{\rho}, \boldsymbol{\xi}) - m_f(\boldsymbol{\rho})\right)\frac{\partial f(\boldsymbol{\rho}, \boldsymbol{\xi})}{\partial \rho_e}\right] \tag{36}$$

In other words, the sensitivities of the mean of the objective function are equal to the mean of the sensitivities of the objective function.

### 4.2 Optimization algorithm

In order to solve the robust optimization problem (34) numerically, the mean and standard deviation of the objective function are estimated by means of a quadrature or sampling method which approximates the expectation operator by a weighted sum:

$$\mathbb{E}[f(\boldsymbol{\rho}, \boldsymbol{\xi})] \approx \sum_{i=1}^{q} w_i f(\boldsymbol{\rho}, \boldsymbol{\xi}_i) \tag{37}$$

where $(\boldsymbol{\xi}_i, w_i)$ are $q$ quadrature points and weights. The sensitivities (35) and (36) are also estimated with the same sampling rule (37). In the examples, we use a Monte Carlo method with 100 samples which are fixed at the start of the optimization. In this case, the samples $\boldsymbol{\xi}_i$ are randomly generated with equal weights $w_i = 1/q$. As every sampling point requires an additional finite element analysis, the computational cost of this approach is relatively high compared to a deterministic optimization. Sampling methods such as the Monte Carlo method, however, are straightforwardly parallelizable since the computations related to one sampling point are independent of those for other sampling points. Therefore, the actual increase in computational time can be strongly reduced.

Alternative uncertainty quantification methods such as Gaussian quadrature (Abramowitz and Stegun 1970), sparse grid quadrature (Smolyak 1963) or stochastic finite elements (Ghanem and Spanos 1991) may be more efficient than the Monte Carlo method when the number of uncertain variables is small. It will be seen in the second and third examples that the number of uncertain variables required to model the vector-valued random field accurately, can become relatively large. In this case, the computational cost of these alternative methods grows rapidly (i.e. the curse of dimensionality), while the accuracy of the Monte Carlo method is independent of the number of uncertain

variables. We should note that more recent uncertainty quantification methods such as the stochastic collocation method (Xiu and Hesthaven 2005) and regression methods (Sudret 2008) can outperform the Monte Carlo method even in high-dimensional problems. Several of these methods have already been applied successfully to robust topology optimization (Chen et al. 2010; Lazarov et al. 2011, 2012; Tootkaboni et al. 2012).

The optimization problem is solved with the Method of Moving Asymptotes (Svanberg 1987). A threshold value $\eta = 0.5$ is applied in the projection step (5) and a continuation scheme on the $\beta$ parameter with a maximum value of 64 is applied in order to avoid ill-conditioning of the problem in the early steps of the optimization process (Sigmund 2007).

Since the samples of the uncertain variables $\boldsymbol{\xi}_i$ are fixed at the beginning of the optimization process, it may be more efficient to compute and store the perturbed filter matrices once and for all at the start of the optimization process (Andreassen et al. 2011).

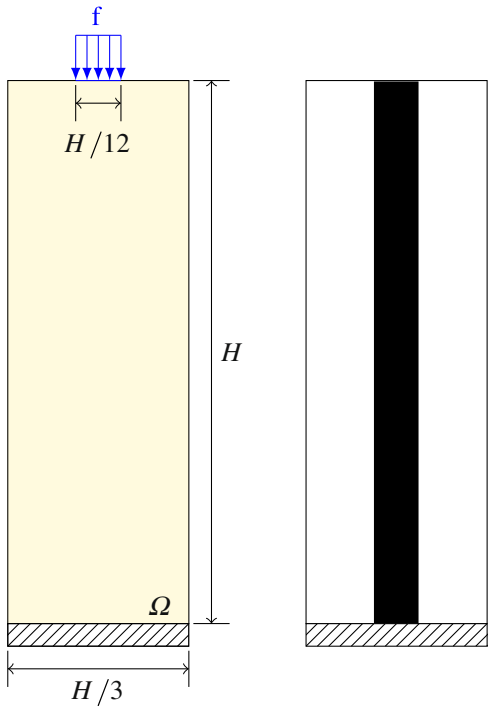


(a) Design domain (b) $\bar{\rho}$

**Fig. 4** Design domain and boundary conditions for a column structure and the deterministic optimal design $\bar{\boldsymbol{\rho}}$

## 5 Examples

### 5.1 Column design

The performance of slender structures is strongly influenced by geometric imperfections due to misalignment. For this reason, the design of a slender column-like structure is considered in this example. The design domain and boundary conditions for the topology optimization problem are shown in Fig. 4a: the design domain $\Omega$ is a rectangular area with a height $H$ and width $H/3$. A distributed load $\mathbf{f}$ with a width of $H/12$ is applied at the top edge. The load per unit length is chosen such that the total load integrates to unity. The bottom edge of the design domain is clamped. The design domain is discretized with $288 \times 96$ equally-sized square finite elements. A penalization parameter $p = 3$, a Young's modulus $E_0 = 1$ and a lower bound $E_{\min} = 10^{-9}$ are used in the SIMP law (1). The filter radius $R$ in the density filter is chosen equal to $0.0215H$ ($= 6.2$ element size). The maximum volume fraction $V_{\max}$ in the minimum compliance problem is chosen equal to 0.25.

The following assumptions are made in the application of the density filter (2). Since the left and right edges of the design domain are free boundaries, no material is present ($\rho = 0$) outside the design domain. At the top and bottom we assume the presence of material ($\rho = 1$) which is a realistic assumption since the column is assumed to be placed on a foundation and to support a beam or floor at the top.

A perfectly straight column is obtained as the solution of the deterministic minimum compliance problem (10) with the use of these parameters. The corresponding element densities $\bar{\boldsymbol{\rho}}$ are shown in Fig. 4b.

In the following step, a random field of geometric imperfections is introduced. In this example, we will only model the horizontal component of the random field (i.e. the component perpendicular to the axis of the column). This means that the vertical component of the random field is equal to zero ($\sigma_{\mathrm{p}_2} = 0$). Furthermore, the correlation length in the horizontal direction is equal to infinity ($l_{\mathrm{c}x} = \infty$). These assumptions lead to a one-dimensional representation of the random field with only a horizontal component $p_1(\mathbf{x}, \theta)$. A standard deviation of $\sigma_{\mathrm{p}_1} = 0.0208H$ is used and a correlation length $l_{\mathrm{c}y} = H$.

The conditional random field approach is used to set the random field equal to zero at the bottom edge of the design domain in order to incorporate the clamped boundary conditions. The conditional random field is described by the conditional covariance function $\tilde{\mathsf{C}}(\mathbf{x}_1, \mathbf{x}_2)$. Figure 5 illustrates the conditioning of the covariance function $C_{\mathrm{p}_1}(\mathbf{x}_1, \mathbf{x}_2)$. The figure shows the covariance functions $C_{\mathrm{p}_1}(\mathbf{x}_1, \mathbf{x}_2)$ and $\tilde{C}_{\mathrm{p}_1}(\mathbf{x}_1, \mathbf{x}_2)$ as a function of the vertical coordinate $y$.

The EOLE method is used to discretize the random field $p_1(\mathbf{x}, \theta)$ with covariance function $\tilde{C}_{\mathrm{p}_1}(\mathbf{x}_1, \mathbf{x}_2)$. Due to the relatively large correlation length of the random field, the EOLE method requires very few points for an accurate approximation of the random field: only six equally

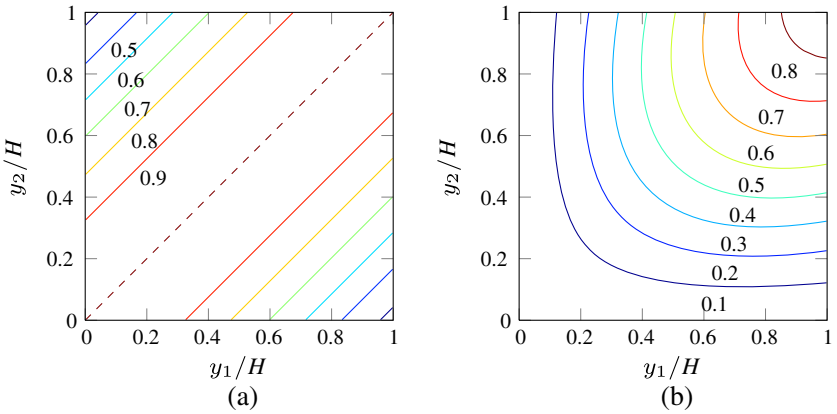


**Fig. 5** Contour plots of **a** the normalized covariance function $C_{p_1}(\mathbf{x}_1, \mathbf{x}_2)/\sigma^2_{p_1}$ and **b** the conditional covariance function $\tilde{C}_{p_1}(\mathbf{x}_1, \mathbf{x}_2)/\sigma^2_{p_1}$ for the random field of horizontal perturbations $p_1(\mathbf{x}, \theta)$ in the column structure

distributed points over the height of the design domain are used. The six modes $\varphi_i(\mathbf{x})$ obtained by the EOLE method are illustrated in Fig. 6 by applying them to the deterministic optimal design. The functions $\varphi_i(\mathbf{x})$ are normalized in Fig. 6 in order to show the difference in shape of the modes. The relative importance of the modes can be analyzed by looking at the mean square error introduced by truncating the EOLE approximation (Li and Der Kiureghian 1993):

$$e^2(\mathbf{x}, r) = \mathbb{E}\left[\left(p_1(\mathbf{x}, \theta) - \sum_{i=1}^{r} \varphi_i(\mathbf{x})\xi_i(\theta)\right)^2\right] = \tilde{\sigma}^2_{p_1}(\mathbf{x}) - \sum_{i=1}^{r} \varphi_i^2(\mathbf{x}) \tag{38}$$

where $\tilde{\sigma}^2_{p_1}(\mathbf{x})$ is the variance of the conditional random field. The relative error $e_{\text{top}}(r) = e(\mathbf{x}_{\text{top}}, r)/\tilde{\sigma}(\mathbf{x}_{\text{top}})$ at the top of the design domain is shown in Fig. 7. Since the error already approaches zero when $r = 3$, the first three modes are the most important and are the only modes taken into account in the robust optimization problem.

The robust optimization problem (34) is solved for four different values of the weighting factor $\omega \in \{0, 0.33, 0.66, 1\}$ in order to investigate the influence of the parameter $\omega$. The solutions are shown in Fig. 8a–d: the designs resemble a tripod-like structure in two dimensions. The two legs of the structure are connected by a thinner cross-bracing which increases the stability of the two separate legs. Comparing the designs obtained with $\omega = 0$ and $\omega = 1$, it can be seen that distance between the legs increases, while the bars in the cross-bracing become thinner for larger values of $\omega$.

As shown by Wang et al. (2011b), the use of a threshold value $\eta = 0.5$ in the projection step (5) does not enforce a length scale into the material phase of the design. This is clearly visible in the designs in Fig. 8b–d where the bars of the cross-bracing are very thin. These results can

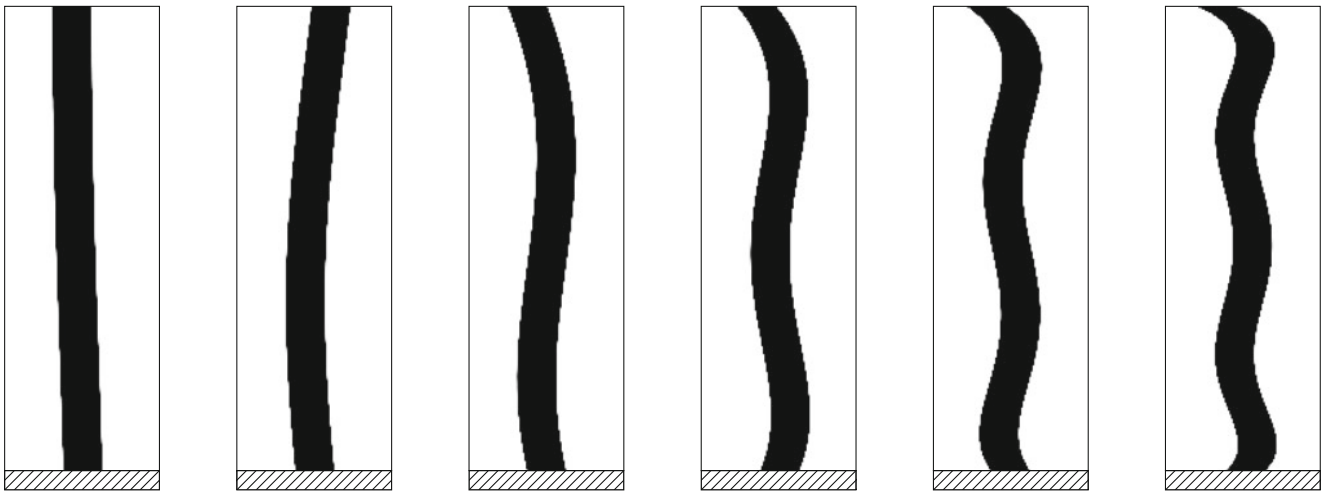

(a) $\varphi_1(\mathbf{x})$ (b) $\varphi_2(\mathbf{x})$ (c) $\varphi_3(\mathbf{x})$ (d) $\varphi_4(\mathbf{x})$ (e) $\varphi_5(\mathbf{x})$ (f) $\varphi_6(\mathbf{x})$

**Fig. 6** Perturbation of the deterministic design by the modes of the EOLE expansion of the Gaussian random field $\mathbf{p}(\mathbf{x}, \theta)$. The modes $\varphi(\mathbf{x})$ are normalized and multiplied by a constant factor = 80 in order to show the difference in shape of the modes

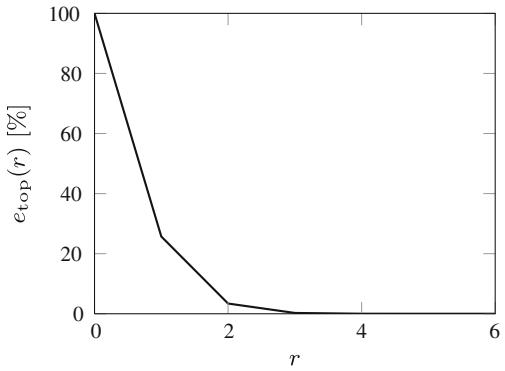


**Fig. 7** The relative error $e_{\text{top}}(r)$ due to truncation of the EOLE expansion as a function of the number of modes in the expansion at the *top* of the design domain

be improved by incorporating the threshold value of the projection step as a uniformly distributed random variable $\eta(\theta) \in \mathcal{U}[a; b]$ (Schevenels et al. 2011). This approach ensures a minimum length scale in the material phase of the nominal design with $\eta = 0.5$ provided that the topology of the design does not change for values of $\eta(\theta)$ in the interval $[a; b]$. The minimum length scale is determined by the filter radius $R$ and the interval $[a; b]$. The problem is solved for the intervals $\eta(\theta) \in \mathcal{U}[0.4; 0.6]$ and $\eta(\theta) \in \mathcal{U}[0.3; 0.7]$. The corresponding length scales in the material phase are approximately equal to $0.0138H$ and $0.0192H$ according to the approach described by Wang et al. (2011b). Figure 8e and f shows the designs obtained by this approach for a value of the parameter $\omega = 1$: black-and-white designs are obtained which contain a minimum length scale in the material phase.

Table 1 summarizes the results for the deterministic and the five robust designs. The nominal performances $f(\boldsymbol{\rho})$ of the designs are compared in the first row: it is clear that the deterministic design performs slightly better than the robust designs in case no geometric imperfections are present.

The values $\hat{m}_f(\boldsymbol{\rho})$ and $\hat{\sigma}_f(\boldsymbol{\rho})$ in Table 1 are the mean and standard deviation estimated by the sampling method in the robust optimization algorithm. An elaborate Monte Carlo simulation with 10,000 samples is used to verify the estimates $\hat{m}_f(\boldsymbol{\rho})$ and $\hat{\sigma}_f(\boldsymbol{\rho})$ and to compare the actual performance of the different designs. The corresponding mean $m_f(\boldsymbol{\rho})$ and standard deviation $\sigma_f(\boldsymbol{\rho})$ are also shown in Table 1. Since the estimates $\hat{m}_f(\boldsymbol{\rho})$ and $\hat{\sigma}_f(\boldsymbol{\rho})$ are very close to the values $m_f(\boldsymbol{\rho})$ and $\sigma_f(\boldsymbol{\rho})$, it can be concluded that using 100 samples in the optimization algorithm is sufficient in this case.

Although the nominal performance of the robust designs is slightly worse, the mean performance $m_f(\boldsymbol{\rho})$ of the robust designs is better than the deterministic design. Furthermore, the robust designs are less sensitive with respect to geometric imperfections which results in much smaller standard deviations $\sigma_f(\boldsymbol{\rho})$.

From the results of Table 1, it can be seen that higher values of $\omega$ lead to more conservative designs. The nominal performance $f(\boldsymbol{\rho})$ increases, while the standard deviation $\sigma_f(\boldsymbol{\rho})$ drops when $\omega$ is increased. At first sight, the mean performances $m_f(\boldsymbol{\rho})$ do not seem to follow the expected trend. For example, $m_f(\boldsymbol{\rho})$ for $\omega = 0$ and $\omega = 0.66$ are larger than $m_f(\boldsymbol{\rho})$ for $\omega = 1$, while it is expected that the mean performance of the design increases when the weighting parameter $\omega$ is increased. This can be attributed to two reasons: (1) inaccuracies due to the estimation of

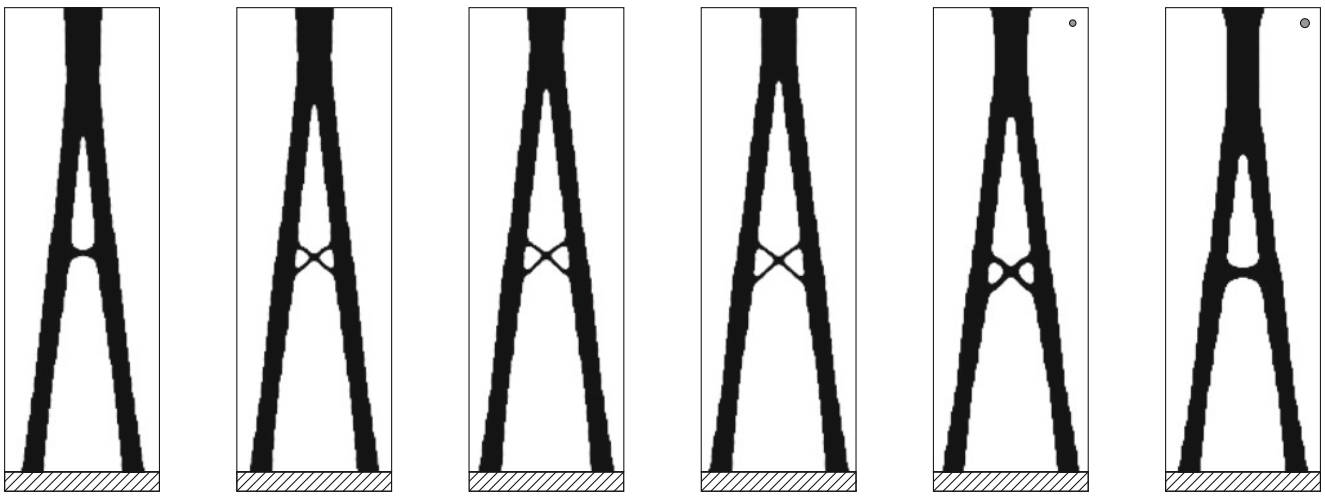


**Fig. 8** Robust optimized designs for the column structure for four values of the parameter $\omega$: **a** $\omega = 0$, **b** $\omega = 1/3$, **c** $\omega = 2/3$, **d** $\omega = 1$. Designs (**e**–**f**) are optimized with $\omega = 1$ and a variable threshold $\eta(\theta) \in \mathcal{U}[0.4; 0.6]$ and $\eta(\theta) \in \mathcal{U}[0.3; 0.7]$ respectively. The minimum length scales imposed in this way are represented by the *circles* in the *top right* corner

**Table 1** Results for the optimized column designs

| | Deterministic | Robust | | | | | |
|---|---|---|---|---|---|---|---|
| $\omega$ | | 0 | 0.33 | 0.66 | 1 | 1 | 1 |
| $\eta$ | 0.5 | 0.5 | 0.5 | 0.5 | 0.5 | $\mathcal{U}[0.4; 0.6]$ | $\mathcal{U}[0.3; 0.7]$ |
| $f(\boldsymbol{\rho})$ | 12.01 | 12.79 | 12.91 | 13.01 | 13.06 | 13.09 | 13.08 |
| $\hat{m}_f(\boldsymbol{\rho})$ | | 13.25 | 13.23 | 13.27 | 13.27 | 13.33 | 13.88 |
| $m_f(\boldsymbol{\rho})$ | 15.04 | 13.32 | 13.27 | 13.32 | 13.31 | 13.48 | 13.76 |
| $\hat{\sigma}_f(\boldsymbol{\rho})$ | | 0.92 | 0.71 | 0.63 | 0.58 | 1.24 | 1.94 |
| $\sigma_f(\boldsymbol{\rho})$ | 3.81 | 0.92 | 0.71 | 0.65 | 0.58 | 1.14 | 1.95 |

the statistics with only 100 Monte Carlo samples in the optimization, and (2) convergence to local minima due to the non-convexity of the optimization problem. It can be seen that a local minimum was found for $\omega = 0$, since the estimate $\hat{m}_f(\boldsymbol{\rho})$ for this case is larger than the one for $\omega = 0.33$. The differences, however, are very small as the relative difference between the highest and the lowest $m_f(\boldsymbol{\rho})$ is less than 2 % which is below the expected accuracy of the 100 Monte Carlo samples. For this reason, it is concluded that the mean performance is relatively independent of the weighting parameter $\omega$ and that an acceptable solution was obtained.

The results for designs e and f of Fig. 8 are shown in the last two columns of Table 1. The solutions of the optimization are also verified by means of a Monte Carlo simulation and $\hat{m}_f(\boldsymbol{\rho})$ and $\hat{\sigma}_f(\boldsymbol{\rho})$ are again good estimates of the statistics $m_f(\boldsymbol{\rho})$ and $\sigma_f(\boldsymbol{\rho})$. It is obvious that the standard deviation of the performance increases by adding the threshold as an uncertain variable to the problem. The designs were also subjected to a Monte Carlo simulation where only misplacement of material was considered as uncertainty. In this case, a mean $m_f(\boldsymbol{\rho}) = 13.43$ and standard deviation $\sigma_f(\boldsymbol{\rho}) = 0.67$ were obtained for design e and $m_f(\boldsymbol{\rho}) = 13.54$ and $\sigma_f(\boldsymbol{\rho}) = 0.81$ for design f. The performances of the designs are almost as good as for the other robust designs while a minimum length scale in the material phase is achieved.

Figure 9 shows the performance (i.e. compliance) of the deterministic design and the robust design e as a function of the first and most important mode of imperfection $\varphi_1(\mathbf{x})$. In case of a perfect system ($\xi_1 = 0$), the robust design has a slightly worse performance. On the other hand, the compliance of the deterministic design increases strongly when imperfections are added, while the performance of the robust design is relatively insensitive to the level of imperfection $\xi_1$.

## 5.2 Cantilever beam

This example illustrates the use of the proposed method in a more general setting by considering the design of a cantilever structure. Figure 10 summarizes the problem description. The design domain $\Omega$ has a height $H$ and length $L = 2.4H$. The left edge of the domain is clamped and a unit point load is applied at the location with a distance $d = 0.12H$ from the right and left edge. Again, the values $p = 3$, $E_0 = 1$ and $E_{\min} = 10^{-9}$ are used in the SIMP law. The maximum volume fraction is 1/4 of the volume of the design domain $\Omega$.

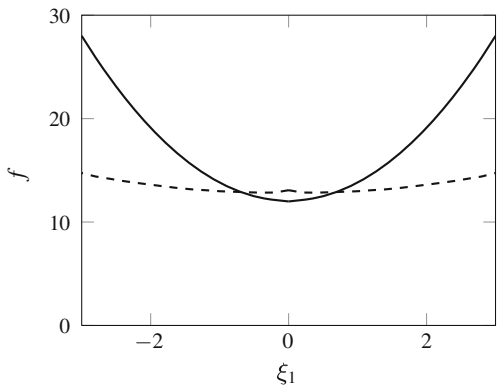


**Fig. 9** Compliance as a function of the first mode of imperfection $\varphi_1(\mathbf{x})$ for the deterministic design of Fig. 4b (*solid line*) and the robust design of Fig. 8e (*dashed line*)

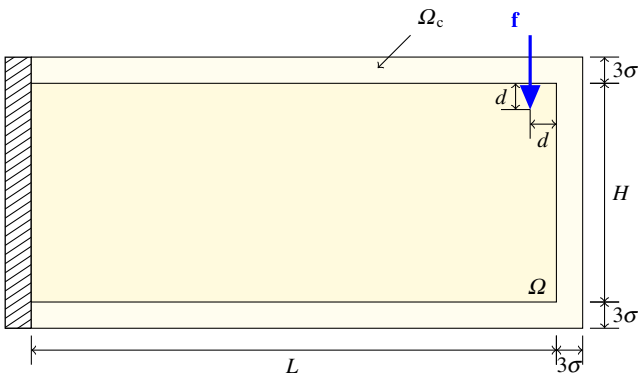


**Fig. 10** Design domain and boundary conditions for the cantilever beam structure

An isotropic random field of perturbations $\mathbf{p}(\mathbf{x}, \theta)$ with $\sigma_{p_1} = \sigma_{p_2} = 0.04H$ and a correlation length $l_c = L/2$ in both directions is used to model the geometric imperfections. In this case, a zero value is imposed on the random field at the left edge of the design domain. This means the random field should be conditioned on a line of known values, while the approach discussed in Section 3.3 is only applicable to a discrete set of points. The actual conditional covariance function is therefore approximated by imposing fixed values of the random field only in a limited number of points on the left edge (Kolanek and Jendo 2008). In this example, 9 equidistant points are used in (21) for the conditional covariance function.

The Eulerian approach of the perturbed filter method has the disadvantage that material can disappear at the edges of the domain. Therefore, it is necessary to add a boundary layer to the computational domain in order to model the perturbations of material realistically at the edges of the domain. This was not necessary in the previous example since the column-like structures are centered in the design domain. The elements in the boundary layer are passive elements in the optimization and their primal densities $\rho_e$ are fixed equal to 0 in order to model the environment around the design. The boundary layer is denoted as $\Omega_c$ in Fig. 10. Since the random field is zero at the left clamped edge, it is unnecessary to introduce additional elements at this side. The width of the boundary layer is chosen such that the probability of material disappearance is sufficiently small. For this reason, a width of $3\sigma$ is used for the boundary layer $\Omega_c$. The design domain and boundary layer are discretized with $252 \times 124$ equally-sized square finite elements. The filter radius is equal to $R = 0.047H$ (or $R = 4.7$ element sizes).

Figure 11 shows the points in the EOLE grid for this problem. Due to the smaller correlation length, more points per unit length are required, but the total number of points $k = 66$ is still very small and the eigenvalue problem (27) poses no problems. A smaller correlation length also implies that more modes are required in the EOLE expansion in order to obtain a good approximation of the random field. Furthermore, the random field in this example is two dimensional and bivariate as opposed to the previous example where a one-dimensional and univariate random field of horizontal perturbations was used. Taking these considerations into account, the number of necessary modes in the EOLE expansion is determined to be equal to 20 based on the mean square error of truncation.

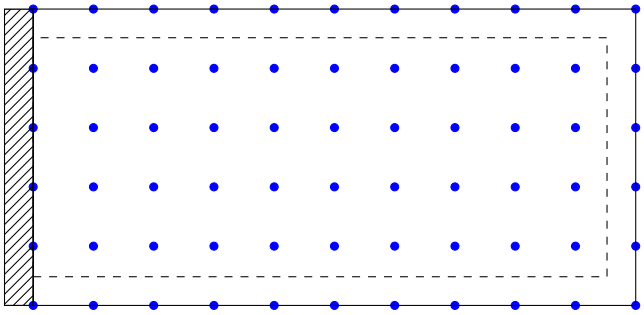

**Fig. 11** Points in the EOLE grid for the random field of imperfections in the cantilever beam design

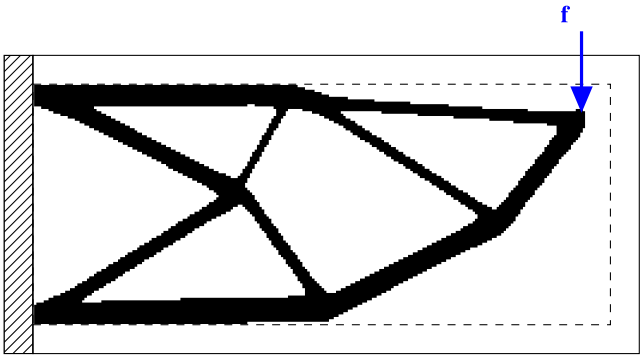


**Fig. 12** Deterministic optimized design for the cantilever beam problem

The design obtained by solving the deterministic optimization problem is shown in Fig. 12. In Fig. 13 the solution of the robust approach with $\omega = 1$ is shown. Compared to the deterministic design, two additional small bars appear in the robust design. These thin bars have a stabilizing effect on the diagonal bar in the middle when imperfections are present. This effect is illustrated in Fig. 14 where the deformation energy per unit volume is shown for a random sample of imperfections. These figures can explain the difference in performance since the compliance is equal to the integral of the deformation energy in the design domain. The deformation in the diagonal and upper right bar is clearly smaller in the robust design.

The results obtained for the two designs are compared in Table 2. Similar to the previous example, the deterministic design performs better in the nominal case. When geometric

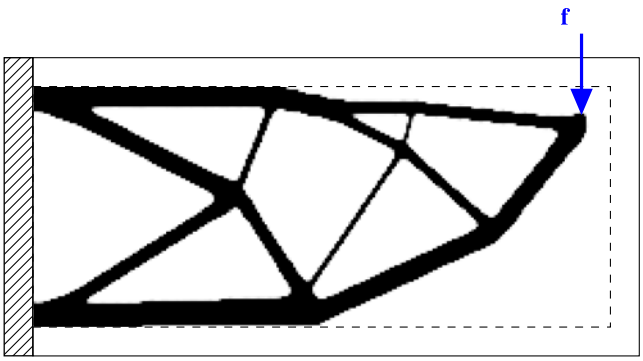


**Fig. 13** Robust optimized design for the cantilever beam problem

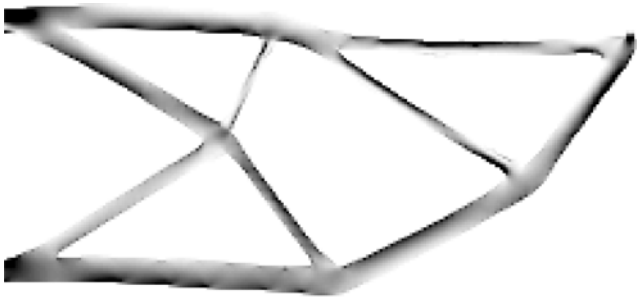

(a) $f = 184.97$

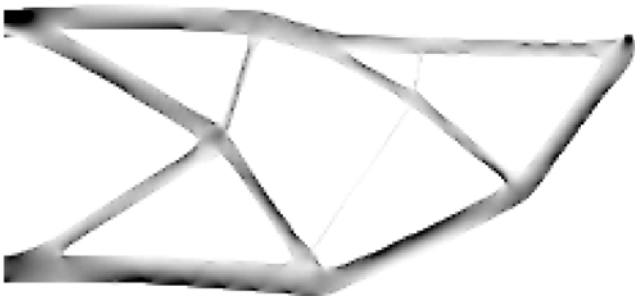

(b) $f = 166.96$

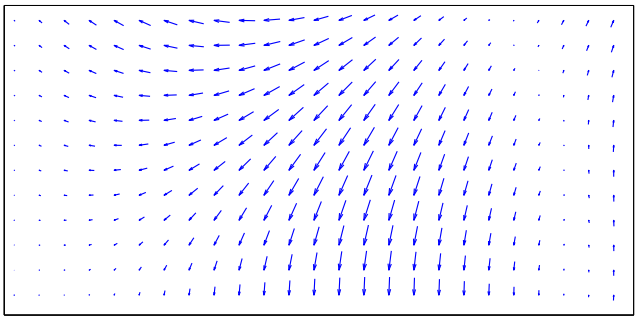

(c) $\mathbf{p}(\mathbf{x}, \theta_i)$

**Fig. 14** **a** Deformation energy stored in the deterministic design and **b** robust design for **c** one realization of the error. The color scale ranges from 0 (*white*) to 0.076 (*black*)

imperfections are present, the mean and standard deviation of the performance of the robust design are better.

In the present example, the optimization was also performed for different values of the weighting parameter $\omega$ in the interval [0; 3]. This, however, did not lead to any significant difference in the final design and corresponding response statistics. For this reason, these results are not included in this paper.

**Table 2** Results for the optimized cantilever designs

| | Deterministic | Robust |
|---|---|---|
| $f(\boldsymbol{\rho})$ | 151.86 | 155.18 |
| $\hat{m}_f(\boldsymbol{\rho})$ | | 155.48 |
| $m_f(\boldsymbol{\rho})$ | 162.77 | 155.62 |
| $\hat{\sigma}_f(\boldsymbol{\rho})$ | | 9.04 |
| $\sigma_f(\boldsymbol{\rho})$ | 10.97 | 9.33 |

### 5.3 Inverter

Misplacement of material is also considered in the benchmark problem of the inverter (Sigmund 1997). The goal is to maximize the output displacement $u_{\text{out}}$ when the input force $f_{\text{in}}$ is applied to the mechanism shown in Fig. 15. The maximum volume fraction is $1/4$ of the volume of the design domain $\Omega$. The input force is equal to $f_{\text{in}} = 2$ and the spring stiffness coefficients are $k_{\text{in}} = 2$ and $k_{\text{out}} = 0.002$. The design domain $\Omega$ is discretized using $240 \times 240$ unit sized finite elements. A filter radius $R = 5.6$ and a projection threshold $\eta = 0.5$ are applied in the density filter.

Misplacement of material is modeled as a two-dimensional random field $\mathbf{p}(\mathbf{x}, \theta)$ with a standard deviation $\sigma = 3$ and correlation length $l_c = L/4$. Furthermore, no misplacement of material occurs at the input and output side of the design domain. A passive layer of elements $\Omega_c$ with a width equal to $3\sigma$ is added to the top and bottom edges of the design domain in order to avoid material from disappearing at these boundaries.

A weighting factor $\omega = 1$ is again applied in the robust optimization. The obtained deterministic and robust optimal designs are shown in Fig. 16a and b. Accounting for misplacement of material has a similar effect as in the cantilever beam problem: additional thin bars appear which

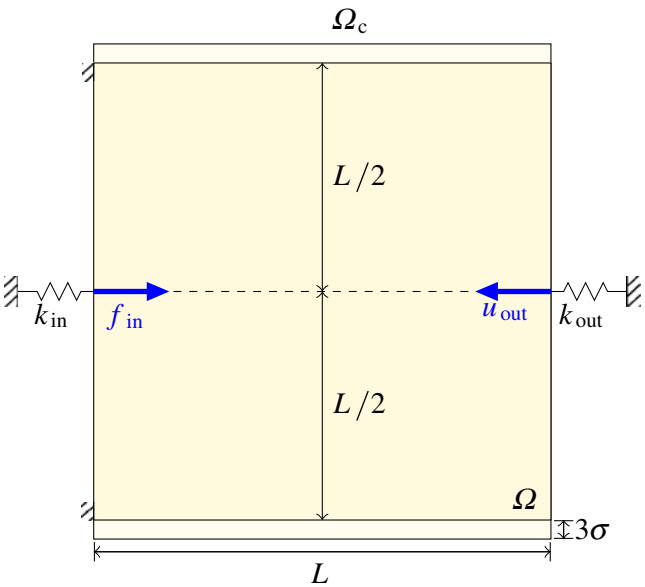


**Fig. 15** Design domain and boundary conditions for the inverter design problem

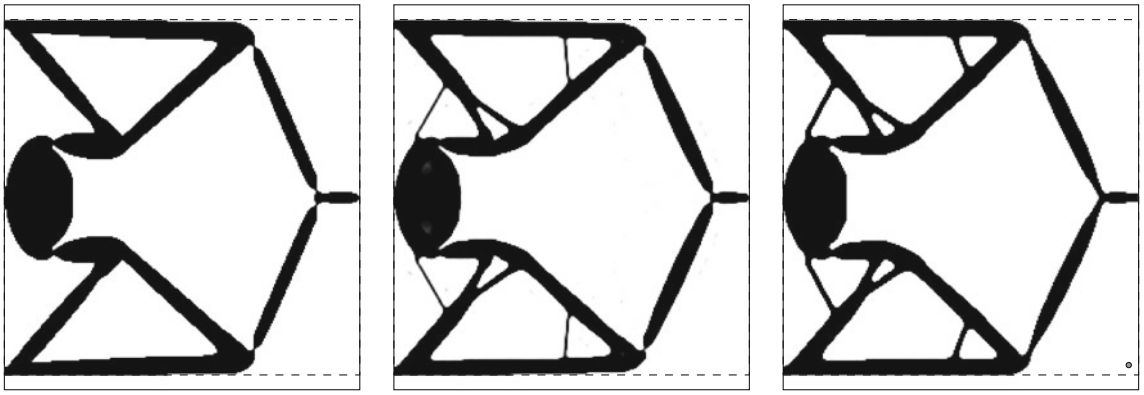

(a) (b) (c)

**Fig. 16** **a** Deterministic design for the force inverter, **b** robust optimized design accounting for material misplacement and **c** robust optimized design accounting for material misplacement and uniform under- and over-etching errors

increase the bending stiffness of the "main" bars. This additional bending stiffness is of importance when the structure is subjected to material misplacement.

The application of a projection threshold $\eta = 0.5$ removes the minimum length scale introduced by the density filter which enables the formation of the thin bars in the robust design in Fig. 16b. Furthermore, the deterministic inverter design contains single node connected hinges and it is clear from Fig. 16b that these are not prevented by taking into account material misplacement. These problems are again solved by including the projection threshold as a random variable in the optimization. Figure 16c shows the design obtained by modeling the projection threshold as a uniformly distributed random variable $\eta(\theta) \in \mathcal{U}[0.4; 0.6]$. The corresponding minimum length scale is equal to 1.77 which is represented by the circle in the lower right corner of the design domain in Fig. 16c. The performance of the designs is compared in Table 3. The statistics for the second robust design (Fig. 16c) in this table are obtained by including the random projection threshold in the calculations. A mean $m_f(\boldsymbol{\rho}) = -2.06$ and standard deviation $\sigma_f(\boldsymbol{\rho}) = 0.05$ are obtained when only material misplacement is considered in the elaborate Monte Carlo simulation. The results show that the nominal performance of the robust designs is slightly worse than the performance of the deterministic design, while the robust designs outperform the deterministic design in the presence of material misplacement errors.

**Table 3** Results for the optimized inverter designs

| | Deterministic | Robust | |
|---|---|---|---|
| $\eta$ | 0.5 | 0.5 | $\mathcal{U}[0.4; 0.6]$ |
| $f(\boldsymbol{\rho})$ | −2.3 | −2.22 | −2.15 |
| $\hat{m}_f(\boldsymbol{\rho})$ | | −2.12 | −2.03 |
| $m_f(\boldsymbol{\rho})$ | −2.05 | −2.12 | −2.03 |
| $\hat{\sigma}_f(\boldsymbol{\rho})$ | | 0.05 | 0.07 |
| $\sigma_f(\boldsymbol{\rho})$ | 0.12 | 0.05 | 0.07 |

## 6 Conclusions and future work

This paper presents a method for incorporating geometric imperfections due to misalignment of material in density based topology optimization. This type of imperfections can deteriorate the performance of slender structures such as columns and braced frames which are often encountered in civil and mechanical applications.

In the proposed method, the translation of material is modeled on a fixed finite element grid by adding a small perturbation to the center of the density filter kernel.

This paper follows a probabilistic approach to robust optimization. This enables the use of random field theory in order to model the spatial variation of the imperfections in the design domain $\Omega$. The uncertainties are propagated in the robust optimization problem by defining the objective function as a weighted sum of the mean and standard deviation of the structural performance subjected to geometric imperfections. In the optimization algorithm, these statistics are estimated by a sampling method (i.e. 100 Monte Carlo samples). Afterwards, the results of the optimization are verified by means of a more elaborate Monte Carlo simulation with 10,000 samples.

Two minimum compliance problems and the design of a compliant mechanism were considered. Although the robust designs obtained by the proposed method have a slightly worse nominal performance compared to their deterministic counterpart, they are less sensitive with respect to geometric imperfections as proved by the results of the extensive Monte Carlo simulation.

The present probabilistic approach can be combined with a random threshold $\eta(\theta)$ (Wang et al. 2011b; Sigmund 2009; Schevenels et al. 2011) in order to obtain designs which are robust with respect to misalignment of material and possess a minimum length scale. The main advantage of the proposed approach compared to the previously proposed threshold based schemes is the ability to model large uncertain variations in the material distribution.

Since the global stability of structures is strongly influenced by imperfections due to misalignment of material, future work will consist of incorporating geometric non-linearities into the robust optimization process.

**Acknowledgements** The research presented in this paper has been performed within the framework of the KU Leuven - BOF PFV/10/002 OPTEC - Optimization in Engineering Center and the NextTop project sponsored by the Villum Foundation. We also acknowledge support via KUL GOA/10/09 MaNet, FWO G.0320.08 (convex MPC), G.0558.08 (Robust MHE), G.0377.09 (Mechatronics MPC), IWT SBO LeCoPro, IUAP P6/04 DYSCO, FP7-EMBOCON (ICT-248940), FP7-SADCO (MC ITN-264735), ERC HIGHWIND (259 166).

## References

Abramowitz M, Stegun I (1970) Handbook of mathematical functions, 9th edn. Dover Publications, New York

Andreassen E, Clausen A, Schevenels M, Lazarov B, Sigmund O (2011) Efficient topology optimization in MATLAB using 88 lines of code. Struct Multidisc Optim 43:1–16

Asadpoure A, Tootkaboni M, Guest J (2011) Robust topology optimization of structures with uncertainties in stiffness—application to truss structures. Comput Struct 89(11–12):1131–1141

Baitsch M, Hartmann D (2006) Optimization of slender structures considering geometrical imperfections. Inverse Probl Sci Eng 14(6):623–637

Ben-Tal A, Nemirovski A (1997) Robust truss topology design via semidefinite programming. SIAM J Optim 7(4):991–1016

Bendsøe M (1989) Optimal shape design as a material distribution problem. Struct Multidisc Optim 1:193–202

Bendsøe M, Sigmund O (2004) Topology optimization: theory, methods and applications, 2nd edn. Springer, Berlin

Beyer H, Sendhoff B (2007) Robust optimization—a comprehensive survey. Comput Methods Appl Mech Eng 196(33–34):3190–3218

Bourdin B (2001) Filters in topology optimization. Int J Numer Methods Eng 50(9):2143–2158

Brittain K, Silva M, Tortorelli D (2011) Minmax topology optimization. Struct Multidisc Optim 45:1–12

Bruns T, Tortorelli D (2001) Topology optimization of non-linear elastic structures and compliant mechanisms. Comput Methods Appl Mech Eng 190(26–27):3443–3459

Chen S, Chen W (2011) A new level-set based approach to shape and topology optimization under geometric uncertainty. Struct Multidisc Optim 44:1–18

Chen S, Chen W, Lee S (2010) Level set based robust shape and topology optimization under random field uncertainties. Struct Multidisc Optim 41:507–524

Ditlevsen O (1996) Dimension reduction and discretization in stochastic problems by regression method. In: Casciati F, Roberts J (eds) Mathematical models for structural reliability analysis, pp 51–138

Eurocode 3 (1994) Design of steel structures. European Commitee for Standardization

Ghanem R, Spanos P (1991) Stochastic finite elements: a spectral approach. Springer-Verlag, New York

Guest J, Igusa T (2008) Structural optimization under uncertain loads and nodal locations. Comput Methods Appl Mech Eng 198(1):116–124

Guest J, Prevost J, Belytschko T (2004) Achieving minimum length scale in topology optimization using nodal design variables and projection functions. Int J Numer Methods Eng 61(2):238–254

Guest J, Asadpoure A, Ha SH (2011) Eliminating beta-continuation from heaviside projection and density filter algorithms. Struct Multidisc Optim 44:443–453

Jalalpour M, Igusa T, Guest J (2011) Optimal design of trusses with geometric imperfections: accounting for global instability. Int J Solids Struct 48(21):3011–3019

JCSS (1999) JCSS probabilistic model code part 3: resistance models. Joint Comittee on Structural Safety

Kogiso N, Ahn W, Nishiwaki S, Izui K, Yoshimura M (2008) Robust topology optimization for compliant mechanisms considering uncertainty of applied loads. J Adv Mech Des Syst Manuf 2(1):96–107

Kolanek K, Jendo S (2008) Random field models of geometrically imperfect structures with "clamped" boundary conditions. Probab Eng Mech 23(2–3):219–226

Kolmogorov A (1956) Foundations of the theory of probability, 2nd edn. Chelsea Publishing Company, New York

Lazarov B, Schevenels M, Sigmund O (2011) Robust design of large-displacement compliant mechanisms. Mech Sci 2(2):175–182

Lazarov B, Schevenels M, Sigmund O (2012) Topology optimization using perturbation techniques taking into account geometric uncertainties. Int J Numer Methods Eng 90(11):1321–1336

Li C, Der Kiureghian A (1993) Optimal discretization of random fields. J Eng Mech 119(6):1136–1154

Rozvany G, Zhou M, Birker T (1992) Generalized shape optimization without homogenization. Struct Multidisc Optim 4:250–252

Schevenels M, Lazarov B, Sigmund O (2011) Robust topology optimization accounting for spatially varying manufacturing errors. Comput Methods Appl Mech Eng 200(49–52):3613–3627

Sigmund O (1997) On the design of compliant mechanisms using topology optimization. Mech Struct Mach 25(4):493–524

Sigmund O (2007) Morphology–based black and white filters for topology optimization. Struct Multidisc Optim 33(4–5):401–424

Sigmund O (2009) Manufacturing tolerant topology optimization. Acta Mech Sin 25:227–239

Sigmund O, Petersson J (1998) Numerical instabilities in topology optimization: a survey on procedures dealing with checkerboards, mesh-dependencies and local minima. Struct Multidisc Optim 16:68–75

Smolyak S (1963) Quadrature and interpolation formulas for tensor products of certain classes of functions. Sov Math, Dokl 4:240–243

Sudret B (2008) Global sensitivity analysis using polynomial chaos expansions. Reliab Eng Syst Saf 93(7):964–979

Sudret B, Der Kiureghian A (2000) Stochastic finite element methods and reliability—a state-of-the-art report. Report UCB/SEMM-2000/08, Department of Civil & Environmental Engineering, University of California, Berkeley

Svanberg K (1987) The method of moving asymptotes—a new method for structural optimization. Int J Numer Methods Eng 24:359–373

Tootkaboni M, Asadpoure A, Guest J (2012) Topology optimization of continuum structures under uncertainty—a polynomial chaos approach. Comput Methods Appl Mech Eng 201–204(1):263–275

Wang F, Jensen J, Sigmund O (2011a) Robust topology optimization of photonic crystal waveguides with tailored dispersion properties. J Opt Soc Am B, Opt Phys 28(3):387–397

Wang F, Lazarov B, Sigmund O (2011b) On projection methods, convergence and robust formulations in topology optimization. Struct Multidisc Optim 43:767–784

Xiu D, Hesthaven JS (2005) High-order collocation methods for differential equations with random inputs. SIAM J Sci Comput 27(3):1118–1139

Xu S, Cai Y, Cheng G (2010) Volume preserving nonlinear density filter based on heaviside functions. Struct Multidisc Optim 41:495–505